POSTER PAPER PRESENTED AT
THE 1994 HYPERVELOCITY IMPACT SYMPOSIUM
HELD AT SANTA FE, NEW MEXICO
OCTOBER 16–19, 1994

# DIMENSIONS AND FRAGMENTATION OF THE NUCLEI OF COMET SHOEMAKER--LEVY 9

ZDENEK SEKANINA

JET PROPULSION LABORATORY
CALIFORNIA INS? ITUTE OF TECHNOLOGY
PASADENA, CALIFORNIA 91109

September 1994

## Abstract

Central regions on the digital maps of 13 nuclear condensations of Comet Shoemaker-Levy 9, obtained with the Planetary Camera of the Hubble Space Telescope on January 27, March 30, and July 4, 1994, have been analyzed with the aim to identify the presence of distinct, major fragments in each condensation, to deconvolve their contributions to the signal that also includes the contribution from a surrounding cloud of dust (modeled as an extended source, using two different laws), to estimate the dimensions of the fragments and to study their temporal variations, and to determine the spatial distributions of the fragments as projected onto the plane of the sky. The deconvolution method applied is described and the results of the analysis are summarized, including the finding that sizable fragments did survive until the time of atmospheric entry, 'His result dots not contradict evidence of the comet's continuing, apparently spontaneous fragmentation, which still went on long after the extremely c1osc approach to Jupiter in July 1992 and which, because of the jovian tidal effects, may even have intensified in the final days before the crash on Jupiter. On plausible assumptions, the largest fragments arc found to have had effective diameters of ~4 km as late as March and even early July 1994. In most condensations, several sizable companion fragments (~1 km across) have been detected within ~1000 km of the projected location of the brightest fragment and the surrounding dust c1ouc1 has been found to be centered on a point that is shifted in the genera] direction of the tail, probably due to effects of solar radiation pressure. Since the developed approach is based on certain premises and involves approximations, the results should be viewed as preliminary and the problem should be a subject of further investigation.

## THE PROBLEM

It is assumed that the observed surface-brightness distribution within each nuclear condensation is a sum of contributions from one or more point sources (major fragments) and an extended source (the surrounding cloud of minor fragments and other particulate material). Let the observed amount of light impinging on a square-shaped pixel in row $X$ and column Y be B(X, Y), in the used analog-to-digital units for the charge-coupled device (ADU). The problem is to find the contributions from the point sources and the extended source to the observed pixel signal distribution by integrating them over all pixels of an imaged field's limited area, which is centered on the brightest pixel, and to determine the dimensions (effective diameter) of each point source from its integrated brightness and an assumed albedo.

## THE POINT SOURCES

The spread function $b_{psf}(x, y)$ of a point source (PSF), expressed in ADU per arcsec$^2$, is approximated by a quasi-Gaussian distribution function:

$$b_{psf}(x, y) = b_* \exp\left[-\left(\frac{x^2+y^2}{2\sigma_{psf}^2}\right)^{\nu_{psf}}\right],$$

where $\sigma_{psf} > 0$ is the PSF's dispersion parameter (in arcsec), $\nu_{psf} > 0$ is a dimensionless constant ($\nu_{psf} = 1$ for the Gaussian function), and $(x^2+y^2)^{1/2} = \rho$ is the angular distance from the PSF's peak, at which the surface brightness $b_{psf}(0, 0) = b_*$. The tots] signal, or the integrated brightness, $I_*$ of a point source is

$$I_* = 2\pi \int_0^\infty \rho\, b_{psf}(\rho)\, d\rho = 2\pi b_* \sigma_{psf}^2 \nu_{psf}^{-1} \Gamma(\nu_{psf}^{-1}),$$

where $I_*$ is in arbitrary intensity units, $b_*$ is in the same units per arcsec$^2$, and l'(z) is the Gamma function of argument $z$:

$$\Gamma(z) = \int_0^\infty t^{z-1} e^{-t} dt \qquad (z > 0).$$

This approximation has been applied to the PSF of the Hubble Space Telescope's (HST) Planetary Camera after its repair in December 1993. In most cases, a 157-pixel array was employed, centered on the brightest pixel of a nuclear condensation and covering a crudely circular area of 15 pixels, or 0.8 arcsec, in diameter. For a point source whose $I_* \simeq 500$ ADU (close to the maximum integrated brightness that has been encountered among the studied fragments), the introduced approximation yields $\sigma_{psf} = 0.0113$ arcsec, $\nu_{psf} = 0.347$, and therefore $I_* = 0.004158\, b_*$. With the Planetary Camera's pixel size of 11 = 0.046 arcsec, the central pixel's signal of ~93.5 ADU implies a peak surface brightness of ~254 ADU/pixel$^2$ or, equivalently, ~1 20,000 ADU/arcsec$^2$. This solution leaves a maximum residual of 3 ADU, which is close to the camera's peak instrumental error, and a mean residual of ±0.86 ADU in the pixel signal. If $\{X_*, Y_*\}$ are the pixel numbers of the I'SF's peak signal for a given point source, the $\{x, y\}$ coordinates of the center of an $\{X, Y\}$ pixel relative to the PSF's peak are:

$$x = \text{II}(X - X_*)$$
$$y = \text{I}](\text{Y} - \text{Y}^*).$$

## THE EXTENDED SOURCE

Two different laws have been considered for the surface-brightness distribution $b_{ext}(\rho)$ of the extended source. Convoluted with the PSF, the laws are assumed in the form:

$$\text{Law A}: \quad b_{ext}(\rho) = \frac{b_0}{1+(\rho/\sigma)^{\nu}}, \qquad \text{Law B}: \quad b_{ext}(\rho) = b_0 \exp\left[-\frac{\rho^2}{2\sigma^2}\right],$$

where $\rho$ is the angular distance from the point of peak surface brightness, $b_{ext}(0) = b_0$, of the extended source, located at a pixel position $\{X_0, Y_0\}$. The dispersion $\sigma$ and the exponent $\nu$ (analogous, in the case of the law B, to $\sigma_{psf}$ and $\nu_{psf}$), as well as $b_0$, $X_0$, and $Y_0$ are constants to be determined by a least-squares differential-correction procedure. The integrated brightness of the extended source is:

$$\text{Law A}: \quad I_0 = 2\pi^2 b_0 \sigma^2 \nu^{-1} \operatorname{cosec}(2\pi/\nu) \text{ for } \nu > 2, \qquad I_0 \to \infty \text{ for } \nu \leq 2.$$

$$\text{Law B}: \quad I_0 = 2\pi b_0 \sigma^2 \nu^{-1} \Gamma(\nu - 1),$$

As in the case of a point source, the $\{x, y\}$ coordinates of the center of an $\{X, Y\}$ pixel relative to the peak of the extended source are

$$x = \Pi(X - X_0)$$
$$y = \Pi(Y - Y_0).$$

## THE SOLUTION

The observed pixel-signal distribution can now be modeled as a sum of the contributions from the $n$ point sources and the extended source, If the pixel location of an $i$th point source is given by $\{(X_*)_i, (Y_*)_i\}$ and its surface-brightness distribution by $b_{psf}^{(i)}(x, y)$, the modeled distribution is calculated by the following integration over each pixel's area:

$$B(X, Y) = \sum_{i=1}^{n} \left\{ \int_{\Pi[X-(X_*)_i-\frac{1}{2}]}^{\Pi[X-(X_*)_i+\frac{1}{2}]} dx \int_{\Pi[Y-(Y_*)_i-\frac{1}{2}]}^{\Pi[Y-(Y_*)_i+\frac{1}{2}]} b_{psf}^{(i)}(x, y)\, dy \right\} + \int_{\Pi(X-X_0-\frac{1}{2})}^{\Pi(X-X_0+\frac{1}{2})} dx \int_{\Pi(Y-Y_0-\frac{1}{2})}^{\Pi(Y-Y_0+\frac{1}{2})} b_{ext}(x, y)\, dy,$$

where the location of the peak of the extended source is allowed to differ from the location of any of the considered point sources, $X_0 \neq (X_*)_i$ and $Y_0 \neq (Y_*)_i, (i = 1, \ldots, n)$.

A solution for $B(X, Y)$ that includes $n$ point sources and an extended source has $(3n+5)$ parameters: $(I_*)_1, \ldots (I_*)_n, (X_*)_1, \ldots (X_*)_n, (Y_*)_1, \ldots (Y_*)_n, b_0, \sigma, \nu$, XO, and $Y_0$. Let the observed distribution $B(X, Y)$ be approximated by a $\mathcal{B}(X, Y)$ array of the summed up contributions from the $n$ point sources and the extended source, calculated with an initial set of values of the (372+-5) parameters. An improved set of values of these parameters, $(I_*)_i + (\Delta I_*)_i, (X_*)_i + (\Delta X_*)_i, (Y_*)_i + (\Delta Y_*)_i (i = 1, \ldots, n)$, bo-I-Abe, $\sigma + \Delta\sigma, \nu +$ Av, $X_0 + \Delta X_0$, and $Y_0 + \Delta Y_0$, results from the equations of condition for the individual parametric corrections. These equations are applied to all pixels that contain information deemed useful for deconvolving the contributions from the various sources. For an {.X, Y} pixel the equation of condition is:

$$B(X,Y) - \mathcal{B}(X,Y) = \sum_{i=1}^{n} \left[ \left( \frac{\partial \mathcal{B}}{\partial I_*} \right)_i (\Delta I_*)_i + \left( \frac{\partial \mathcal{B}}{\partial X_*} \right)_i (\Delta X_*)_i + \left( \frac{\partial \mathcal{B}}{\partial Y_*} \right)_i (\Delta Y_*)_i \right]$$
$$+ \frac{\partial \mathcal{B}}{\partial b_0} \Delta b_0 + \frac{\partial \mathcal{B}}{\partial \sigma} \Delta \sigma + \frac{\partial \mathcal{B}}{\partial \nu} \Delta \nu + \frac{\partial \mathcal{B}}{\partial X_0} \Delta X_0 + \frac{\partial \mathcal{B}}{\partial Y_0} \Delta Y_0.$$

With the partial derivatives calculated numerically, the application of a least-scluarcs differential-correction procedure allows one to iterate the solution until it has converged. If noise in the input data impedes the convergence, a more: cautious approach should be applied by solving for only some of the parameters at any one time and to expand the number of parameters to $(3n + 5)$ gradually ant] only after the convergence is reached when solving for fewer than the full number of parameters. This approach is particularly appropriate in the early stages of the iteration procedure, before the solution has "settled" around the optimum parametric values, or when the convergence has been slow.

The experience with the calculations whose results arc described in the next section suggests that the following general approach should be employed in analyzing the signs] distribution from the data charts of the observed images:

**Step** 1 begins with the assumption that the observed signal is due entirely to the extended source, One may have to start with solving for only some of the source's parameters but eventually does so for all five of them to find an initial solution and the distribution of pixel-brigl]tncss residuals.

**Step** 2 starts with an inspection of the distribution of residuals from the available solution. For a given pixel sample (mostly 157 pixels centered on the brightest one), the resulting mean residual is compared with that for the PSF of a comparable peak signal, usually equal to about, or less than, $\pm 1$ ADU. If the mean residual is significantly greater than $\pm 1$ ADU or if the distribution displays clumps of residuals of slightly elevated (positive) values, an improved solution is deemed desirable and the analysis continues. If the distribution of residuals and the mean residual indicate a satisfactory fit to the data set, the analysis is terminated. Almost invariably, a continuation of the analysis in these cases would result in progressively growing convergence difficulties, whose presence is yet another impetus for the procedure's termination.

**Step** 3, initiated when the fit by the solution from Step 2 is deemed unsatisfactory, involves the introduction of a new point source to improve yhe distribution of pixel-brightness residuals. The location of this source is approximated by the coordinates of the pixel of the maximum positive residual exhibited by the available distribution. Since the total brightness of this source is at this stage unknown, its initial value is merely a guess; zero is one of feasible options that can be employed.

**Step** 4 is the search for an improved solution. It includes (a) the determination of the parameters for an expanded set of sources using the iterative least-squares differential-correction procedure and (b) the calculation of a ncw distribution of pixel-brightness residuals and a new mean residual. If this mean residual is still unacceptably large, another point source is introduced and the procedure starting with Step 2 is repeated.

In addition to the test based on a mean residual, other statistically diagnostic criteria can be used to see whether the detected sources do indeed exist, For example, a result is customarily considered meaningful when it is determined with a formal precision of $>3\sigma$.

## THE RESULTS

The described approach has been applied to digital maps of the brightness distribution on the images of several nuclear condensations of Comet Shoemaker–Levy 9, as observed with the HST Planetary Camera. Tables 1-G and Figs. 1-3 present the results of these calculations. The effective diameters of the fragments are determined from their $R$ magnitudes (derived from the ADU units and tile exposure time with the use of a transformation formula), assuming a geometric albedo of 0.04 and a phase coefficient of 0.035 mag/deg. On these assumptions, the formal 1 $\sigma$ error in the calculated diameters is typically $\pm 0.1$ to $\pm$ 0.2 km, but, realistically, diameters $\lesssim$1 km can be at best only marginally detected.

For each of the nuclear condensations F, G, H, N, $1'_1$, $P_2$, $Q_1$, $Q_2$, R, S, T, U, and V, Table 1 compares the laws A and B for the assumed brightness distribution in the extended source in terms of the effective diameter of the largest fragment and the number of detected companions, based on the HST observations made on January 27, 1994. It is noted that no point source is needed to fit most satisfactorily the brightness distribution of the condensation V when the law A is applied; this is indicated by assigning a value of $<<1$ km to the effective diameter of the largest fragment. When the law B is used, the detection is apparently also less than marginal, only at a $2\sigma$ level for, the integrated brightness. The comparisons of columns 2 and 3 and also of columns 4 and 5 lead to the obvious conclusion that the results are for all practical purposes independent of the adopted law. However, the table shows that in the employed set of 157 pixels the mean residual from the law A is often better and never worse than from the law B, so the law A has subsequently been adopted in Tables 2 and 3.

Table 2 lists the effective diameter of the largest fragment and the number of companions detected in the HST digital maps of the comet's images taken on January 27,

TABLE 1

Comparison of Effective Diameters of Largest Fragments and Numbers of Companions Derived From HST Observations Made on Jan. 27, 1994 Using Two Different Laws for Surface Brightness Distribution in Extended Source.

| Condensation | Largest object's effective diameter (km) | | Number of detected companions | | Mean residual (ADU) | |
|---|---|---|---|---|---|---|
| | Law A | Law B | Law A | Law B | Law A | Law B |
| F | 2.3 | 2.3 | 1 | 1 | $\pm$0.96 | $\pm$0.97 |
| G | 4.3 | 4.4 | 4 | 4 | $\pm$1.26 | $\pm$1.28 |
| H | 3.3 | 3.2 | 3 | 2 | $\pm$1.19 | $\pm$1.25 |
| N | 1.6 | 1.6 | 0 | 0 | $\pm$0.79 | $\pm$0.79 |
| $P_1$ | 1.3 | 1.3 | 2 | 2 | $\pm$0.96 | $\pm$0.98 |
| $P_2$ | 2.4 | 2.4 | 5 | 3 | $\pm$0.88 | $\pm$0.97 |
| $Q_1$ | 4.0 | 4.0 | 5 | 5 | $\pm$1.16 | $\pm$1.17 |
| $Q_2$ | 3.2 | 3.2 | 2 | 2 | $\pm$0.91 | $\pm$0.94 |
| R[a] | 2.7 | 2.8 | 0 | 0 | 40.97 | $\pm$1.02 |
| R[b] | 2.7 | 2.5 | 0 | 0 | $\pm$1.19 | $\pm$1.23 |
| S | 3.6 | 3.6 | 8 | 6 | $\pm$1.09 | $\pm$1.18 |
| T | 1.4 | 1.4 | 1 | 1 | $\pm$0.80 | $\pm$0.81 |
| U | 1.3 | 1.3 | 0 | 0 | $\pm$0.69 | $\pm$0.69 |
| V | $\ll$1 | $\lesssim$1 | 0 | 0 | $\pm$0.83 | $\pm$0.83 |

[a] From image on Q frame.
[b] From image on S frame.

TABLE 2

Effective Diameters of Largest Fragments and Numbers of Companions From HST Observations (Extended Source Subtracted Using Law A).

| Condensation | Largest object's effective diameter (km) | | | Number of detected companions | | |
|---|---|---|---|---|---|---|
| | Jan. 27 | Mar. 30 | Jul. 4 | Jan. 27 | Mar. 30 | Jul. 4 |
| F | 2.3 | 2.1 | ... | 1 | 1 | ... |
| G | 4.3 | 3.7 | ... | 4 | 3 | ... |
| H | 3.3 | ... | ... | 3 | ... | ... |
| N | 1.6 | 1.4 | ... | 0 | 0 | ... |
| $P_1$ | 1.3 | 0.6 | ... | 2 | 0 | ... |
| $P_2$ | 2.4 | 1.4 | ... | 5 | 4 | ... |
| $Q_1$ | 4.0 | 2.9 | 3.9 | 5 | 2 | 5 |
| $Q_2$ | 3.2 | 1.5 | 2.5 | 2 | 3 | 3 |
| R | 2.7 | 2.1 | ... | 0 | 2 | ... |
| S | 3.6 | 2.5 | ... | 8 | 6[a] | ... |
| T | 1.4 | ... | ... | 1 | ... | ... |
| U | 1.3 | 1.0 | ... | 0 | 0 | ... |
| V | <<1 | ... | ... | 0 | ... | ... |

[a] Effective diameter of the largest companion is 2.3 km.

March 30, and July 4, 1994. The data in columns 2-4 suggest that there is no systematic variation in the dimensions with time. Even though it appears that the calculated sizes of most of the fragments were smaller in March than in January, the data for the fragments $Q_1$ and $Q_2$, observed on all three dates, show that by July their dimensions recovered to close to their January values and that perhaps the variations could be primarily a rotational effect of strongly irregular shape. Likewise, the numbers of detected companions, in columns 5-7, do not exhibit any significant trend. It is highly probable that there is no relationship among the various companions detected at different times and that the relatively large numbers of these companions present evidence for an apparently continuing disintegration of the large fragments in numerous discrete events. The dots indicate the absence of digital maps for the respective condensations on the given dates.

Table 3 summarizes the apparent $R$ magnitudes of all detected fragments and their calculated effective diameters. Dots indicate the unavailability of the relevant data for this study, while hyphens show the absence of additional fragments in the available data. A tendency is noticed for each condensation to possess one fragment whose size dominates. Exceptions are the condensations $P_1$ and perhaps also $P_2$ on January 27 and S on March 30, for which the first two largest fragments are of similar size. However, only the fragments of the last two condensations are significantly above the detection limit. It will be of interest to correlate any possible multiple impact events of the individual condensations with evidence from Table 3.

A set of the solutions and the quality of their fit to the observed pixel-brightness distribution as the number of the assumed point sources increases is exemplified in Table 4. The listed solutions refer to the nucleus condensation H observed on January 27, 1994, are optimized over a set of 157 pixels centered on the brightest one, and the extended source's brightness distribution is approximated by the law A.

TABLE 3

Apparent Magnitudes and Effective Diameters of Fragments Derived From HST Observations (Extended Source Subtracted Using Law A).

| Condensation | Fragment | Apparent $R$ magnitude | | | Effective diameter (km) | | |
|---|---|---|---|---|---|---|---|
| | | Jan. 27 | Mar. 30 | Jul. 4 | Jan. 27 | Mar. 30 | Jul. 4 |
| F | 1 | 24.65 | 24.23 | ... | 2.3 | 2.1 | ... |
| | 2 | 26.09 | 25.47 | ... | 1.2 | 1.2 | ... |
| | 3 | – | 25.50 | ... | | 1.2 | ... |
| G | 1 | 23.28 | 23.08 | ... | 4.3 | 3.7 | ... |
| | 2 | 25.23 | 24.94 | ... | 1.8 | 1.6 | ... |
| | 3 | 25.7'3 | 25.00 | ... | 1.4 | 1.5 | ... |
| | 4 | 25.87 | 25.48 | ... | 1.3 | 1.2 | ... |
| | 5 | 26.39 | | ... | 1.0 | | ... |
| 11 | 1 | 23.89 | ... | ... | 3.3 | ... | ... |
| | 2 | 25.29 | ... | ... | 1.7 | ... | ... |
| | 3 | 26.34 | ... | ... | 1.1 | ... | ... |
| | 4 | 26.64 | ... | ... | 0.9 | ... | ... |
| N | 1 | 25.37 | 25.10 | ... | 1.6 | 1.4 | ... |
| 1'] | 1 | 25.89 | 26.96 | ... | 1.3 | 0.6 | ... |
| | 2 | 26.30 | | ... | 1.1 | | ... |
| | 3 | 26.48 | | ... | 1.0 | – | ... |
| $P_2$ | 1 | 24.54 | 25.13 | ... | 2.4 | 1.4 | ... |
| | 2 | 24.88 | 25.89 | ... | 2.1 | 1.0 | ... |
| | 3 | 25.65 | 26.28 | ... | 1.4 | 0.8 | ... |
| | 4 | 25.99 | 26.38 | ... | 1.2 | 0.8 | ... |
| | 5 | 26.25 | 26.92 | ... | 1.1 | 0.6 | ... |
| | 6 | 26.44 | | ... | 1.0 | | ... |
| $Q_1$ | 1 | 23.42 | 23.57 | 23.27 | 4.0 | 2.9 | 3.9 |
| | 2 | 24.80 | 25.43 | 24.96 | 2.1 | 1.2 | 1.8 |
| | 3 | 25.51 | 26.22 | 25.26 | 1.5 | 0.9 | 1.6 |
| | 4 | 25.70 | | 25.52 | 1.4 | – | 1.4 |
| | 5 | 25.72 | .. | 25.69 | 1.4 | | 1.3 |
| | 6 | 26.22 | | 26.56 | 1.1 | | 0.9 |
| $Q_2$ | 1 | 23.95 | 24.97 | 24.25 | 3.2 | 1.5 | 2.5 |
| | 2 | 25.32 | 26.16 | 24.98 | 1.7 | 0.9 | 1.8 |
| | 3 | 25.62 | 26.46 | 25.47 | 1.5 | 0.8 | 1.4 |
| | 4 | -. | 26.50 | 25.81 | | 0.6 | 1.2 |
| R | 1 | 24.26 | 24.25 | ... | 2.7 | 2.1 | ... |
| | 2 | -. | 25.75 | ... | | 1.1 | ... |
| | 3 | – | 26.04 | ... | | 0.9 | ... |
| S | 1 | 23.69 | 23.92 | ... | 3.6 | 2.5 | ... |
| | 2 | 25.54 | 24.06 | ... | 1.5 | 2.3 | ... |
| | 3 | 25.83 | 25.62 | ... | 1.3 | 1.1 | ... |
| | 4 | 25.98 | 25.72 | ... | 1.2 | 1.1 | .,. |
| | 5 | 26.04 | 26.13 | ... | 1,2 | 0.9 | ... |
| | 6 | 26.14 | 26.15 | ... | 1.2 | 0.9 | ... |
| | 7 | 26.15 | 26.17 | ... | 1.1 | 0.9 | ... |
| | 8 | 26.18 | | ... | 1.1 | | ... |
| | 9 | 26.56 | – | ... | 1.0 | | ... |
| T | 1 | 25.72 | ... | ... | 1.4 | ... | ... |
| | 2 | 27.16 | ... | ... | 0.7 | ... | ... |
| U | 1 | 25.92 | 25.80 | ... | 1.3 | 1.0 | .,. |

TABLE 4

Set of Solutions for the Nuclear Condensation H, Observed by the HST'S Planetary Camera on January 27, 1994, As a Function of the Number of Assumed Fragments (Law A).

| Number of point sources assumed | Mean residual (ADU) | Point source | | | | Extended source | | | | |
|---|---|---|---|---|---|---|---|---|---|---|
| | | Id. | $I_*$ ($10^3$ADU) | $X_*$ (pixels) | $Y_*$ (pixels) | $b_0$ ($10^5$ADU/arcsec$^2$) | $\sigma$ (arcsec) | $\nu$ | $X_0$ (pixels) | $Y_0$ (pixels) |
| 0 | ±1.99 | ... | .. | ... | ... | 0.462 ± 0.022 | 0.056 ± 0.005 | 1.22 ± 0.04 | 10.22 ± 0.03 | 10.18 ± 0.03 |
| 1 | ±1.44 | a | 0.233 ± 0.014 | 10.12 ± 0.05 | 9.62 ± 0.03 | 0.240 ± 0.012 | 0.119 ± 0.009 | 1.38 ± 0.06 | 10.35 ± 0.04 | 10.67 ± 0.05 |
| 2 | ±1. 27 | a | 0.259 ± 0.012 | 10.25 ± 0.03 | 9.60 ± 0.02 | 0.216 ± 0.010 | 0.127 ± 0.010 | 1.30 ± 0.06 | 10.51 ± 0.05 | 10.81 ± 0.06 |
| | | *b* | 0.068 ± 0.010 | 8.78 ± 0.12 | 10.43 ± 0.07 | | | | | |
| 3 | ±1.23 | a | 0.265 ± 0.011 | 10.26 ± 0.03 | 9.60 ± 0.02 | 0.212 ± 0.009 | 0.130 ± 0.009 | 1.31 ± 0.06 | 10.51 ± 0.05 | 10.86 ± 0.06 |
| | | *b* | 0.070 ± 0.009 | 8.77 ± 0.11 | 10.41 ± 0.07 | | | | | |
| | | *c* | 0.019 ± 0.006 | 11.32 ± 0.29 | 5.16 ± 0.40 | | | | | |
| 4 | ±1.19 | a | 0.272 ± 0.012 | 10.30 ± 0.03 | 9.62 ± 0.03 | 0.208 ± 0.009 | 0.128+ 0.009 | 1.26 ± 0.06 | 10.57+ 0.06 | 10.97 ± 0.07 |
| | | *b* | 0.075 ± 0.009 | 8.77 ± 0.10 | 10.48 ± 0.07 | | | | | |
| | | *c* | 0.021 ± 0.006 | 11.34 ± 0.25 | 5.28 ± 0.28 | | | | | |
| | | *d* | 0.028 ± 0.008 | 8.92 ± 0.35 | 8.68 ± 0.21 | | | | | |

The match is seen to improve dramatically after the first point source (identified by the letter a and equal to the major fragment 3.3 km in diameter; cf. Tables I-3) has been introduced in the solution, indicating that its existence cannot be ignored. If, for example, the extended source's convoluted variation with radial distance from the peak-brightness point extended all the way to the central pixel, the value of the dispersion $\sigma$ would have to amount to only a small fraction of the pixel size, that is, $\sigma << 0.046$ arcsec, in contradiction to the optimum value. Further improvements in the fit are apparent as contributions from additional point sources, identified by the letters $b$- d, have been allowed for. As expected, the calculated contribution from the extended source gradually decreases as the number of introduced point sources increases. This drop is considerable after the first point source, but tapers off as more point sources are included. No converging solution could be found that would involve more than four point sources. The calculated integrated brightness of each point source appears to increase with the number of the assumed sources, but the rate of increase also tapers off as their number increases. The calculated positions of the point sources are seen to be, within the errors, rather consistent and essentially independent of the solution. The letter identification of the fragments has been introduced to emphasize the order in which they nave Lccn included in the solution, in contrast to their numerical identification used in Table 3 and organized in the order of decreasing size. For the condensation II, the correspondence between the two classifications is obviously: 1 = a, 2 = $b$, 3 = $d$, and 4 = $c$.

The gradual improvement in the quality of the fit to the observed signal distribution of the condensation II is apparent from Tables 5 and 6, which list four maps of the brightness residuals in tile 157 pixels. Table 5 presents the maps for the solutions with no and one point source assumed, while Table 6 for two and four point sources assumed. The position of the brightest pixel is always given by $X$ = Y = 10 pixels and the residuals are in the ADU units Highlighted in each map is the most conspicuous clump of positive residuals, indicating another potential point source. It is noted that the prominence of the clump diminishes from an area of four neighboring pixels with a peak residual of +9 ADU and a minimum residual of +2 ADU in the map for the solution in which only the extended source was assumed, to an area of only two neighboring pixels with a peak residual of +3 ADU and the minimum residual of + 2 ADU. Also noted in the map for the solution with no assumed point source is a strong systematic. trend, from generally negative residuals in the region $X$ <10 pixels, Y <10 pixels to generally positive residuals in the region $X$ >10 pixels, Y >10 pixels. This asymmetry appears to be brought about by a slight displacement of the extended source, relative to the brightest point source, by about +0.3 pixel in the $X$ coordinate ancl by a little more than +1 pixel in the Y coordinate. As shown below, this direction is c1osc to the projected antisunward direction and the extended source's displacement is likely to be due to solar radiation pressure effects on the particulates in the dust cloud, whose model the extended source represents,

Figure 1 depicts the best model for the brightness distribution near the center of the condensation II, observed with the Planetary Camera on January 27, 1994. The model includes the contributions from four point sources (the fragments a, $b$, $c$, and $d$) and an extended source (the surrounding dust cloud), With the model's parameters listed in 'J'able 4, the contributions to the total signal of the brightest pixel are calculated to amount to $51\frac{1}{2}$ percent from the fragment a, $43\frac{1}{2}$ percent from the dust cloud, 4 percent from $b$, and 1 percent from $d$. It is noted that the peak-hrightncss area of the dust cloud appears in the figure only as a modest bulge on the slope of the PSF of the fragment a.

TABLE 5

Distribution of Pixel-Brightness Residuals (in ADU) for the Nuclear Condensation H, Observed by the HST'S Planetary Camera on January 27, 1994, As a Function of the Number of Assumed Fragments.

| Number of point sources assumed = O (Mean residual = ±1.99 ADU) | | | | | | | | | | | | | | | | |
|---|---|---|---|---|---|---|---|---|---|---|---|---|---|---|---|---|
| X (pixels) | Y (pixels) | | | | | | | | | | | | | | | |
| | 3 | 4 | 5 | 6 | 7 | 8 | 9 | 10 | 11 | 12 | 13 | 14 | 15 | 16 | 17 | |
| 3 | | | | | | | 0 | −1 | o | | | | | | | 3 |
| 4 | | | | | | −1 | −3 | -4 | −1 | −1 | o | J-3 | | | | 4 |
| 5 | | | | | −2 | −2 | -3 | −2 | −2 | −3 | −1 | o | −2 | | | 5 |
| 6 | | | | O | − 2 | − 2 | - 2 | − 4 | − 3 | O | 0 | −1 | +1 | +1 | | 6 |
| 7 | | | −1 | 0 | −1 | −3 | −2 | −3 | −1 | +1 | −1 | O | 0 | 0 | +2 | 7 |
| 8 | | | 0 | 0 | −3 | −2 | −3 | −1 | 0 | +2 | +1 | +2 | +1 | +1 | + 3 | 8 |
| 9 | | +1 | −1 | + 2 | − 2 | −1 | -1 | +2 | +2 | +1 | o | + 4 | +1 | +1 | +1 | +1 | 9 |
| 10 | | +1 | −1 | 0 | − 3 | − 2 | −3 | +9 | +1 | - 6 | −1 | +1 | + 2 | +4 | +2 | +2 | 10 |
| 11 | | +1 | o | +1 | 0 | - 4 | −4 | +4 | −2 | -3 | - f - | 3 | + 2 | 4 | - 3 | + 4 | + 3 | +3 | 11 |
| 12 | | | −1 | +1 | 0 | - 2 | −1 | -1 | −2 | +1 | o | +2 | +3 | +3 | +1 | | 12 |
| 13 | | | +2 | −1 | −1 | −1 | −1 | o | 0 | −1 | +1 | +1 | 0 | + | 1 | + 2 | | 13 |
| 14 | | | | o | o | − | 1 | o | 0 | −1 | −1 | +1 | +2 | −1 | +1 | | | 14 |
| 15 | | | | | − | 1 | 0 | +1 | 0 | −1 | +2 | +1 | 0 | +2 | | | | 15 |
| 16 | | | | | | o | - f - | 2 | +1 | +1 | +3 | +1 | +2 | | | | | 16 |
| 17 | | | | | | | +2 | +1 | +1 | | | | | | | | | 17 |

| Number of point sources assumed = 1 (Mean residual = ±1.44 ADU) | | | | | | | | | | | | | | | | |
|---|---|---|---|---|---|---|---|---|---|---|---|---|---|---|---|---|
| X (pixels) | Y (pixels) | | | | | | | | | | | | | | | |
| | 3 | 4 | 5 | 6 | 7 | 8 | 9 | 10 | 11 | 12 | 13 | 14 | 15 | 16 | 17 | |
| 3 | | | | | | | o | -1 | 0 | | | | | | | 3 |
| 4 | | | | | | 0 | − | 2 | − | 3 | - | 1 | - | 1 | 0 | + 2 | 4 |
| 5 | | | | | −1 | −1 | −2 | −2 | -2 | −3 | −1 | −1 | − 2 | | | 5 |
| 6 | | | | +1 | −1 | −2 | −1 | −3 | −2 | 0 | 0 | −2 | 0 | 0 | | 6 |
| 7 | | | 0 | +1 | 0 | −2 | −1 | −2 | o | +1 | −1 | −1 | o | −1 | +2 | 7 |
| 8 | | | 0 | +1 | −1 | −1 | −1 | +1 | +1 | +3 | +1 | +1 | o | 0 | +2 | 8 |
| 9 | | +1 | 0 | +3 | −1 | +1 | +1 | +2 | +4 | +3 | −1 | +3 | 0 | −1 | 0 | 0 | 9 |
| 10 | | +1 | 0 | +1 | −2 | 0 | − | 2 | - | 1 | - | 2 | − | 1 | − | 3 | − | 1 | 0 | +2 | +1 | +1 | 10 |
| 11 | | +1 | +1 | +2 | +2 | -2 | −3 | +3 | +2 | −1 | +1 | O | +1 | +2 | +2 | +2 | 11 |
| 12 | | | 0 | +2 | +1 | o | 0 | 0 | −1 | +1 | −2 | 0 | +1 | +1 | o | | 12 |
| 13 | | | +2 | o | − | 1 | o | 0 | 0 | 0 | − | 2 | 0 | 0 | − | 2 | 0 | +1 | | 13 |
| 14 | | | | +1 | o | - | 1 | 0 | +1 | −1 | −2 | 0 | +1 | −2 | o | | | 14 |
| 15 | | | | | 0 | +1 | +1 | 0 | −1 | +1 | +1 | −1 | +1 | | | | | 15 |
| 16 | | | | | | +1 | +2 | +1 | o | +3 | +1 | +1 | | | | | | 16 |
| 17 | | | | | | | +2 | +1 | 0 | | | | | | | | | 17 |

TABLE 6

Distribution of Pixel-Brightness Residuals (in ADU) for the Nuclear Condensation H, Observed by the HST's Planetary Camera on January 27, 1994, As a Function of the Number of Assumed Fragments.

| Number of point sources assumed = 2 (Mean residual = ±1.27 ADU) | | | | | | | | | | | | | | | | | Number of point sources assumed = 4 (Mean residual = ±1.19 ADU) | | | | | | | | | | | | | | | | |
|---|---|---|---|---|---|---|---|---|---|---|---|---|---|---|---|---|---|---|---|---|---|---|---|---|---|---|---|---|---|---|---|---|
| X (pixels) | Y (pixels) | | | | | | | | | | | | | | | | Y (pixels) | | | | | | | | | | | | | | | | x (pixels) |
| | 3 | 4 | 5 | 6 | 7 | 8 | 9 | 10 | 11 | 12 | 13 | 14 | 15 | 16 | 17 | | 3 | 4 | 5 | 6 | 7 | 8 | 9 | ICI | 11 | 12 | 13 | 14 | 15 | 16 | 17 | |
| 3 | | | | | | | o–1 | o | | | | | | | | 3 | | | | | | | o–1 | o | | | | | | | | 3 |
| 4 | | | | | | O – 2 - 3 – l – 1 | | | | | | | O - ? - 2 | | | 4 | | | | | | 9 – 2 – 3 – 1 – 1 | | | 0 | +2 | | | | | 4 |
| 5 | | | | −1 | –I | –2 | −1 | –I | –2 | –1 | o | –2 | | | | 5 | | | | –1 | –1. | –2 | −1 | −1 | –2 | −1 | 0 | -2 | | | | 5 |
| 6 | | | | +1 | -1–1 | | O–3–2 | | O | | 0-1 | | 0 | | 0 | 6 | | | | +1 | 0 | −1 | 0 | −2 | −1 | +1 | +1 | −1 | 0 | 0 | | 6 |
| 7 | | | 0 | +1 | o | – 2 | o | – 2 | 0 | +1 | −1 | o | 0 | −1 | +1 | 7 | | | 0 | +1 | o–2 | | o-1 | | 0 | +2 | o | 0 | 0 | −1 | +1 | | 7 |
| 8 | | | 0 | +1 | – 1 | o | 0 | +1 | −1 | +1 | +1 | +2 | o | | 0+2 | 8 | | | | +1 | +1 | −1 | o | −1 | +1 | −1 | +1 | +1 | +2 | o | 0 | + 2 | | 8 |
| 9 | +1 | | 0+3 | | 0 | +1 | +2 | +3 | O | 0 | −1 | +3 | 0 | −1 | O | 0 | +1 | o | +3 | | 0 | +1 | 0 | 0 | 0 | −1 | 0 | +3 | 0 | −1 | o | −1 | 9 |
| 10 | -f-I | o | +1 | –I | +1 | −1 | −1 | 0 | +1 | −2 | o | | 0 | +2 | 0 +1 | 10 | +1 | o | 0 | −2 | +1 | −1 | o | 0 | +1 | −2 | o | | 0+2 | 0 | +1 | | 10 |
| 11 | +1 | +1 | +3 | +2 | –2 | -2 | +1 | | 0 | −1 | +1 | | 0 | +1 | +2 | +1 +1 | +1 | o | 0 | | 0 | −2 | −2 | +1 | −1 | −1 | +1 | 0 | +1 | +2 | +1 | +1 | 11 |
| 12 | | | 0 | +2 | +1 | o | 0 | +1 | –1 | | +1 | –2 | o | +1 | +1 | –1 | | | −1 | o | 0 | | 0 | +1 | +1 | 0 | +1 | −2 | 0 | +1 | +1 | −1 | | 12 |
| 13 | | | +2 | o | 0 | 0 | 0 | +1 | | o–2 | | | o–l–2–1 | | | o | | | +2 | −1 | −1 | 0 | +1 | +1 | +1 | −1 | O – 1 | | - 2 - 1 | | o | | 13 |
| 14 | | | | 0 | o | – 1 | 0 | +1 | −1 | −2 | o | | o | – 3 - 1 | | | | | 0 | 0 | | 0 | +1 | +1 | −1 | −1 | o | | o - 3 - I | | | | 14 |
| 15 | | | | -I | o | +1 | 0 | −1 | +1 | | o | – 1 | | o | | | | | | o | +1 | +1 | | o | −1 | +1 | | o–1 | | o | | | 15 |
| 16 | | | | | 0+2 | | o | | 0+2 | | 0 | +1 | | | | 16 | | | | | 0 | +2 | | o | | 0+2 | | 0 | +1 | | | | 16 |
| 17 | | | | | | | | +1 | +1 | 0 | | | | | | 17 | | | | | | | | | +1 | +1 | 0 | | | | | | 17 |

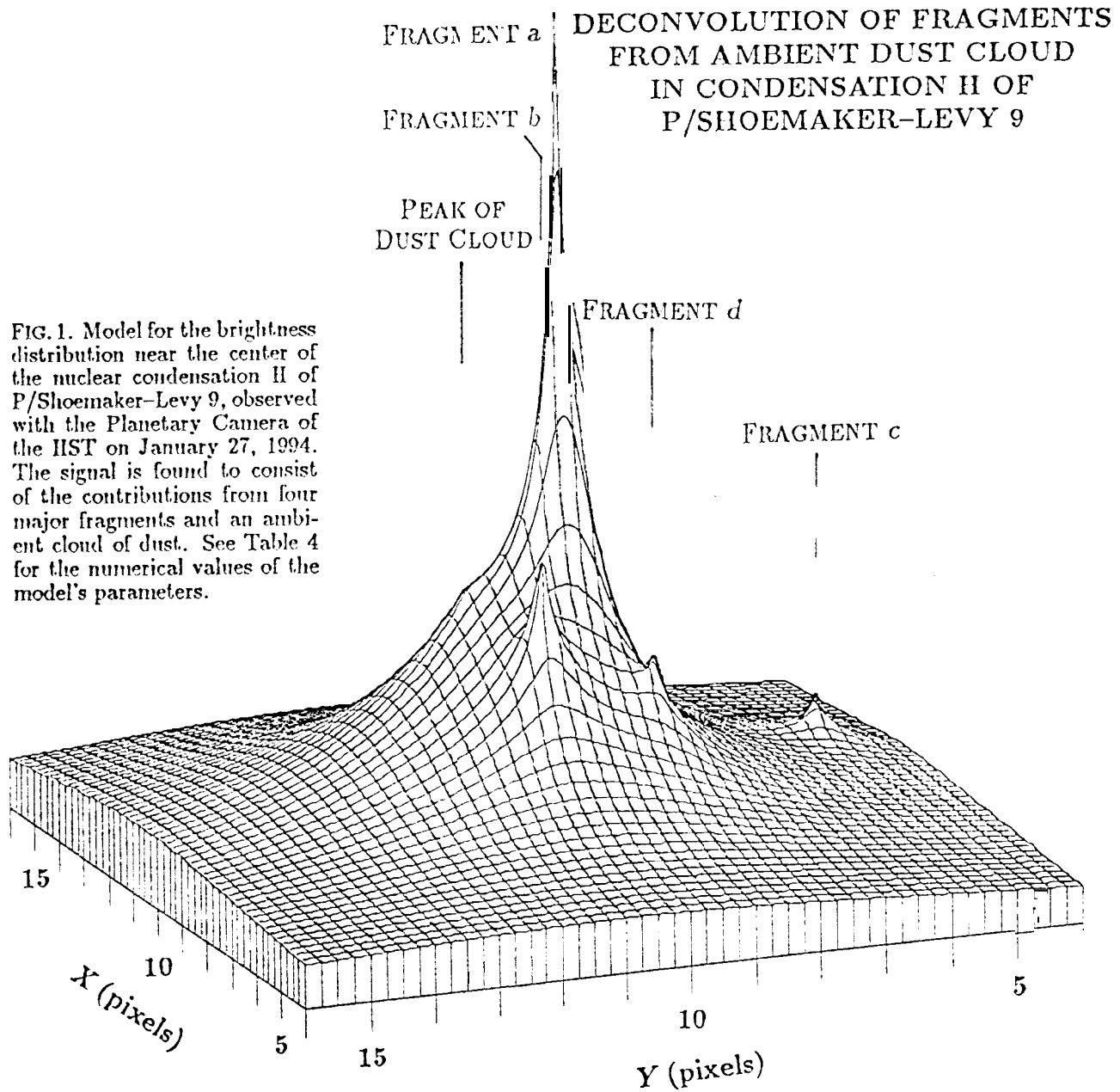


FIG. 1. Model for the brightness distribution near the center of the nuclear condensation H of P/Shoemaker–Levy 9, observed with the Planetary Camera of the HST on January 27, 1994. The signal is found to consist of the contributions from four major fragments and an ambient cloud of dust. See Table 4 for the numerical values of the model's parameters.

Finally, Figs. 2 and 3 show the projected spatial distributions of the companions and the dust cloud's peak relative to the brightest fragment in each condensation on, respectively, January 27 and March 30, 1994. The projected distances involved in the two figures arc typically a fcw hundred kilometers, up to ~1000 km. The dust clouds in most condensations are sewn to be centered on points that are located generally to the west of the brightest fragments, which is the direction of the tails and which is consistent with the presence of a slight cumulative effect clue to solar radiation pressure from the time of tidal breakup in July 1992. This predicted direction is 273° on January 27 and 269° on March 30, 1994. Also noticeable is a persistent lineup of several companions in the condensation S to the south of the brightest fragment. A plume of material was repeatedly reported to extend in this direction on visually inspected high-resolution images.

## CONCLUSIONS

The results of this investigation indicate that prolific fragmentation of the comet's nucleus continued for a considerable period of time after the initial tidal breakup in July 1992, so that the dimensions of the individual fragments were time dependent. This process of fragmentation, while essentially continuous taken stochastically, appears to have proceeded—at least in its early stages, involving large, kilcnnctcr-sized fragments- in the form of discrete events, which can readily explain the repeatedly observed instances of sudden, sllort-term brightening of the various condensations. There is little doubt that, as a result of the fragmentation events recurring over and over again, many of the objects eventually disintegrated to the extent that they could no longer be detected individually even on the digital maps of the condensations and merely contributed to the surrounding dust cloud. However, available evidence shows that, in spite of the progressive fragmentation, one dominant fragment persisted in most condensations. The most striking exception to this rule is provided by the condensation S, in which two shout equally bright. fragments, separated by some 160 km in projection onto the plane of the sky ancl each of a calculated effective diameter of ~2.5 km, were detected by analyzing the digital map of the condensation's image taken on March 30, 1994.

Although the dimensions of individu al fragments must obviously have diminshed with time, no systematic rate of decrease could be established from the available data. Shortly before their crash on Jupiter, the largest fragments were still found to have effective diameters of ~4 km, comparable with those derived by Weaver *et al.* (] 994) from the HST observations in July 1993 and consistent with the dimensions of the parent nucleus of the comet proposed by Sekanina *et al.* (1 994). The integrated decrease in the dimensions of the large fragments appears to be substantially less significant than variations in the projected cross-sectional area associated with the rotation of these highly irregular objects. The dust clouds associated with the condensations show signs of slight effects of solar radiation pressure, which should be expected for assemblages dominated by centimeter-sized particulates.

Since the employed approach is based on certain premises (such as the prescribed laws for the extended source and the empirical fit to the tabulated PSF for the point sources) and involves certain approximations (such as neglect of the sky background), the presented results should be viewed as preliminary. It is certain that attention will remain focussed on the problem of analysis of the 11 ST digital maps as onc of the most hopeful avenues for determining the dimensions of Comet Shoemaker- Levy 9, perhaps the most unusual comet ever observed.

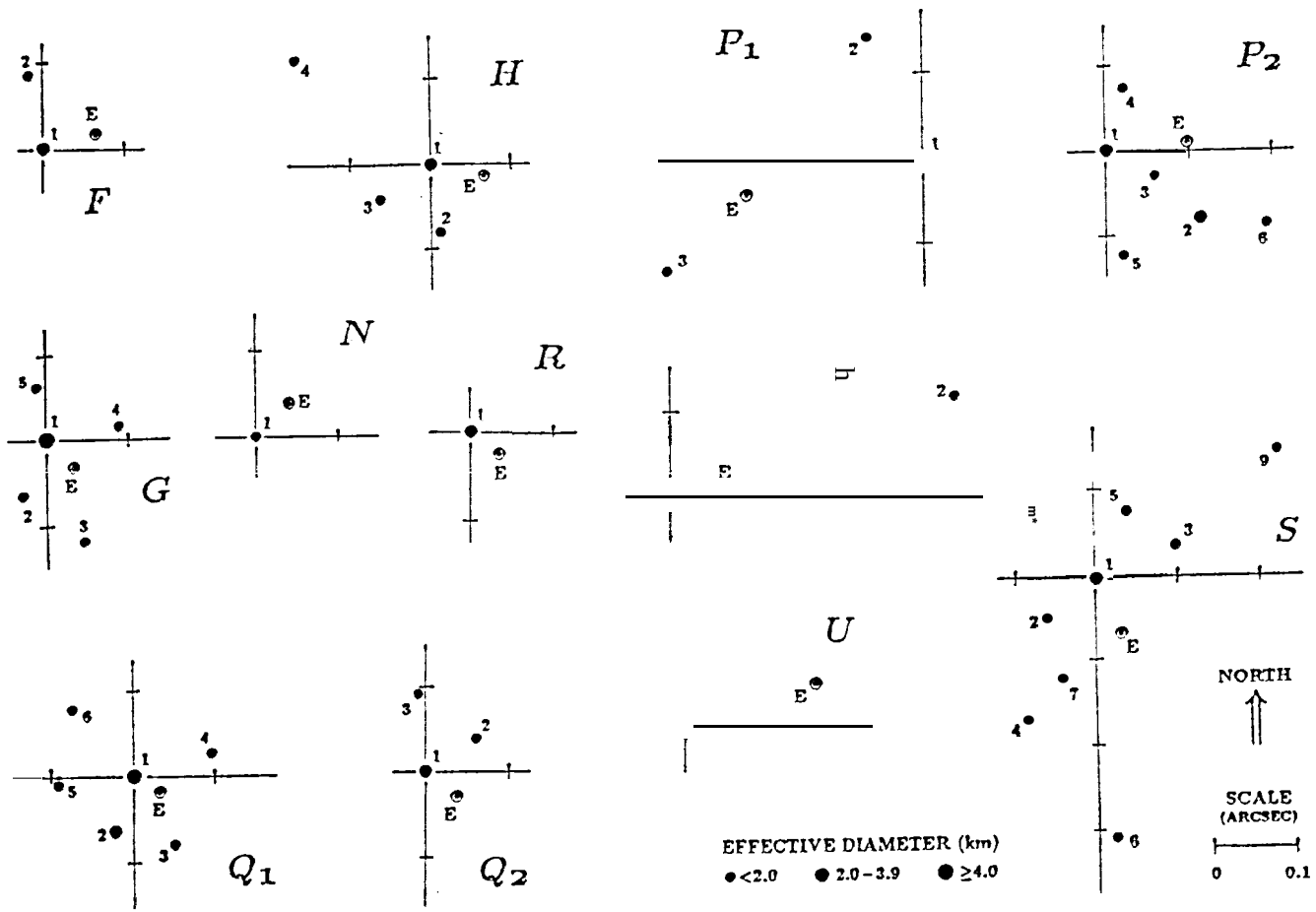


FIG. 2. Projected separations of the companion fragments and the brightness peak of the dust cloud (the extended source) from the brightest fragment in the nuclear condensations F, G, H, N, $P_1$, $P_2$, $Q_1$, $Q_2$, R, S, T, and U, based on the observations made with the HST Planetary Camera on January 27, 1994 and calculated from the analysis of the pixel-brightness distribution near the center of each condensation. The offsets are in the equatorial coordinate system and the angular scale is shown near the bottom-right corner of the figure. At the comet's distance, 0.1 arcsec corresponds to a projected distance of 390 km. The individual fragments are plotted as solid circles of different sizes, correlated with their derived dimensions and are identified by numbers in the order of their decreasing size (Table 3). The locations of the extended-source peaks are plotted as circled dots identifed with the letter E. It is noted that in most condensations the dust cloud is centered on a point that is located in a generally westerly direction from the brightest fragment. Also, several fragments in the condensation S are approximately lined up toward the south.

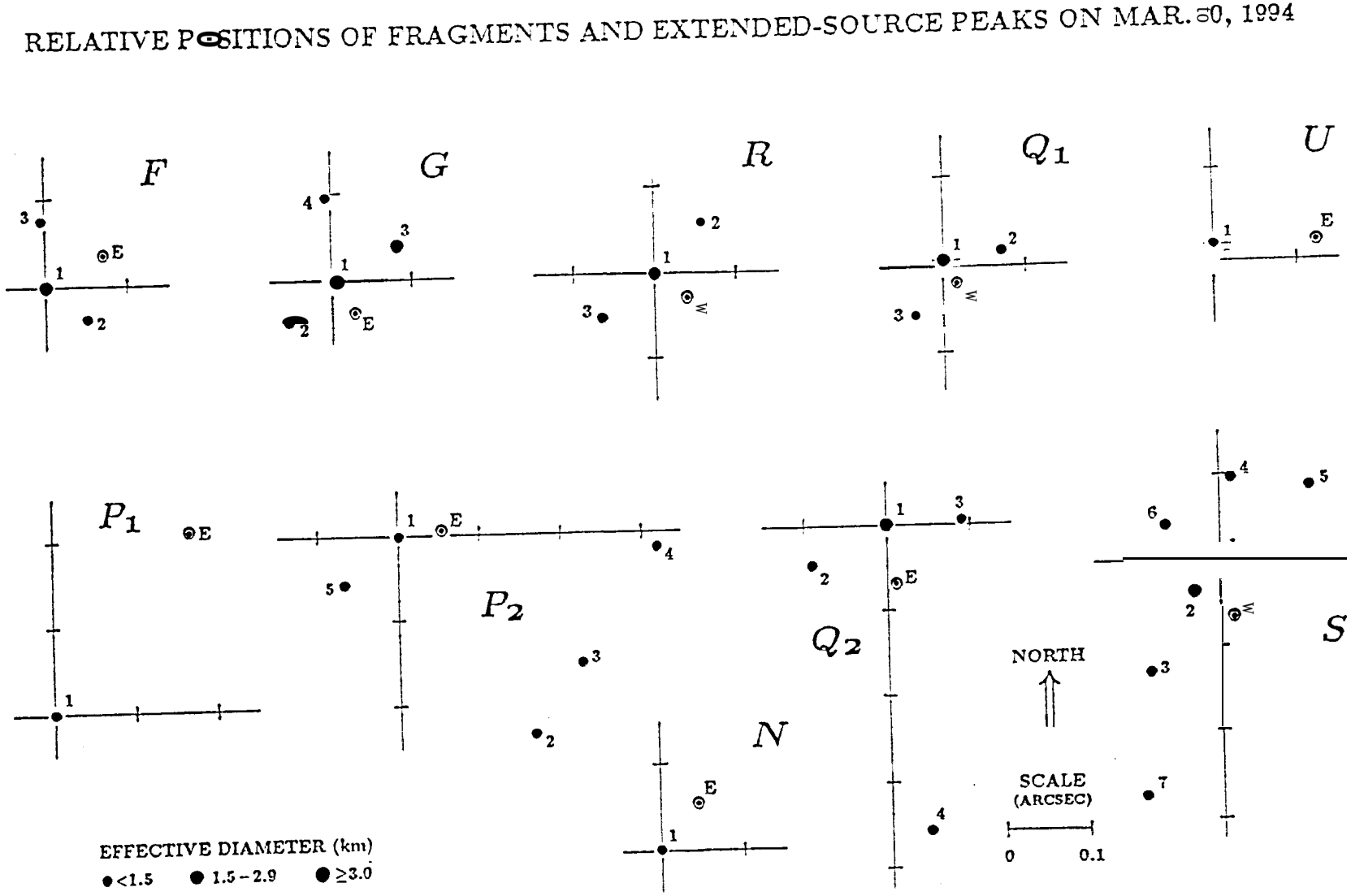


FIG. 3. Projected separations of the companion fragments and the brightness peak of the dust cloud (the extended source) from the brightest fragment in the nuclear condensations F, G, N, $P_1$, $P_2$, $Q_1$, $Q_2$, R, S, and U, based on the observations made with the HST Planetary Camera on March 30, 1994 and calculated from the analysis of the pixel-brightness distribution near the center of each condensation. For more description, see the caption to Fig. 2. At the comet's distance, 0.1 arcsec corresponds to a projected distance of 327 km. It is noted that, as in Fig. 2, the dust cloud is centered on a point generally to the west of the brightest fragment. Several fragments in the condensation S are still lined up toward the south.

## ACKNOWLEDGEMENTS

I thank H. A. Weaver for providing the digital maps for the nuclear condensations of Cornet Shoemaker-Lcwy 9, which were secured with the Planetary Camera of the HST and are analyzed in this study, and for his comments on the approach I have developed. This work is based on observations made with the NASA/ESA Hubble Space Telescope obtained at the Space Telescope Science institute (Sri'ScI), which is operated by the Association of Universities for Research in Astronomy, Inc., under contract with the National Aeronautics and Space Administration. This research was carried out by the Jet Propulsion Laboratory, California, Institute of Technology, under contract with the NASA. partial support was provided by the NASA through Grants GO-5021 and GO-5624 from the STScI.

## REFERENCES

Sekanina, Z., Chodas, P. W., and Yeomans, D. K. (1994). Tidal Disruption and the Appearance of Periodic Comet Shoemaker-Levy 9. *Astronomy &* Astrophysics 289, 607-636.

Weaver, 11. A., Feldman, 1'.11., A'Hearn, M. F., Arpigny, C., Brown, R. A., Helin, E., F., Levy, D. 11., Marsden, B. G., Meech, K. J., Larson, S. M., Nell, K. S., Scotti, J. V., Sekanina, Z., Shoemaker, C. S., Shoemaker, E. M., Smith, T. 13., Storrs, A. D., Yeomans, D. K., and Zellner, B. (1994). Hubble Space Telescope Observations of Comet P/Shoemaker-Levy 9 (1993c). *Science* 263, 787-791.